High precision in-situ measurement of speed of sound in hydraulic systems

Nigel Johnston

University of Bath

Abstract

An existing ISO standard frequency-domain method for measurement of speed of sound in a hydraulic pipeline is enhanced and extended in this paper to include in-situ measurement of pressure transducer calibration factors. Transducer mounting stresses are shown to cause variations in the calibration factors, and the proposed method can be used to eliminate these uncertainties, consequently improving the accuracy of the speed of sound. 95% confidence ranges in the speed of sound of less than +/-0.1% have been achieved, and such high precision cannot be achieved by other practical methods. The method can also been extended to estimate viscosity and mean flow velocity, but accuracy is less good.

Novel time-domain versions of the method are introduced. These may be valuable for real-time monitoring, and changes in speed of sound or calibration factor can be tracked with minimal delay. Some examples showing the effect of sudden aeration are presented; a sudden drop in speed of sound is apparent.

Keywords

Hydraulics, fluid power, speed of sound, calibration, wave propagation

Introduction

The speed of sound is an important property of fluid in a hydraulic line. It influences the dynamic behaviour of the system, the resonant frequencies, and the magnitude of water hammer waves. Accurate knowledge of the value is often needed, in order to be able to model and predict the behaviour of hydraulic systems accurately, and to be able to measure and model the hydro-acoustic properties of components, for example the flow ripple and source impedance of a pump [1]. In digital switched hydraulic systems, accurate tuning of the switching frequency may be needed for optimum efficiency [2], and this depends on the speed of sound.

The speed of sound depends on the fluid density and isentropic tangent bulk modulus, as well as on the compliance of the pipe wall and on any entrained air bubbles. Fluid manufacturers do not always provide sufficient information about the bulk modulus; it varies with temperature and pressure, and the isothermal secant bulk modulus is often quoted instead of the isentropic tangent value. The pipe wall compliance effect depends on the pipe clamping/mounting arrangements as well as the wall properties. The presence and quantity of air bubbles is extremely difficult to predict, and a very small quantity of air bubbles can cause an extremely large reduction in the speed of sound. For these reasons the speed of sound is very difficult to predict accurately.

Margolis and Brown [3] developed a method to measure the speed of sound and attenuation of sinusoidal disturbances in turbulent flow, and showed comprehensive results as functions of frequency and Reynolds number. This very detailed work used three pressure transducers equally spaced in a coiled tube 137m in length. Bolleter [4] used a similar method using three equally spaced

pressure transducers in a 1.25m long tube, a much more convenient and practical arrangement suitable for in-situ testing, but neglected viscous friction effects and frequency variations in the speed of sound. Johnston and Edge [5] included frictional effects, and extended the method to work with unequally spaced transducers. This is beneficial as some methods for measurement of flow ripple, impedance and transfer matrices [1, 6, 7, 8, 9] also require three unequally spaced pressure transducers, to avoid ill-conditioned equations when the transducers are spaced a multiple of a half wavelength apart. Johnston and Edge's method was adopted as one of two alternatives in ISO 15086-2:2000 [10], in which it is recommended for use "at any time when the speed of sound is to be measured under the effective working conditions in a system", as it is well suited for in-situ use under normal working flow and pressure conditions.

ISO 15086-2 [10] also provides an alternative method, based on anti-resonance in a tube. This method is mathematically simpler than the three-transducer method and only requires two transducers and less precise calibration. However it requires a specially designed side branch tube with a bleed-off valve that must be closed during the speed of sound test, so cannot be applied under true in-situ through flow conditions; it is possible that the speed of sound may change when the flow is stopped, due to the fluid cooling or bubbles settling out.

Other methods are based on measuring the wave delay between two pressure transducers, using cross correlation techniques [11, 12]. These methods are simple and can be applied in-situ provided that sufficient high frequency periodic, random or transient pressure ripple excitation is available. The accuracy of Karjalainen et al's [11] and Yu et al's [12] results was unclear, but is likely to be strongly dependent on having sufficient high frequency excitation and a high sample rate. The cross correlation method has some similarities with the proposed method; both are based on pressure measurements in a tube, and both can be implemented in-situ in a through-flow pipeline without special end conditions. Both methods are based on adjusting delays in order to minimise or maximise a function. The cross correlation method is simple in principle, but results may be affected by reflections, though this was not reported to have caused problems by Karjalainen or Yu et al. Conversely, in the proposed method the effect of reflections is eliminated mathematically, but the mathematical analysis is more complex.

Yu and Kojima [13] provided an excellent review of existing methods, and proposed a method that can be used to measure the speed of sound in test components which may be rigid lines, compliant pipelines or flexible hoses. This was based on the measurement of the transfer matrix of the test component, using two rigid reference pipelines each with two pressure transducers. If the test component is a rigid pipeline and identical to the two reference pipelines, the speed of sound in the reference pipelines can be measured. Alternatively if the speed of sound in the reference pipelines is known, the speed of sound in the test component can be measured. ISO 15086-3 [14] provides a similar means for measuring the transfer matrix of a component, but specifies three transducers in each reference pipeline so that the speed of sound in the reference pipelines can be measured using the method specified in ISO 15086-2 [10] and described here.

In this paper, the three-transducer frequency domain method for measuring speed of sound, developed by the author [5] is extended for improved accuracy and for high-precision estimation of calibration factors. The estimation of other parameters such as viscosity is also investigated. The method is extended to a time-domain approach, with a view to applications such as real-time condition monitoring. Some examples of results are given and the value of such results explored.

Experimental test method

The methods proposed here are based on three pressure transducers situated in a uniform rigid pipeline, distances Δx_1 and Δx_2 apart, with no restrictions, cavities or branches between the transducers, as shown in figure 1. All results presented in this paper were obtained from experimental data obtained using this test rig.

Experiments were performed using an automotive power steering pump as the flow and pressure source, with Petronas Tutela GI/R power steering fluid (ISO VG 22). Tests were performed for pressures between 10 bar and 60 bar and temperatures between 30°C and 60°C. The system was loaded using a simple restrictor valve. Pressure transducers were PCB 112A21 miniature piezoelectric pressure transducers, with a range of 69 bar (1000 psi), natural frequency of 250 kHz and diaphragm diameter of 5.5 mm. These were fitted in steel blocks, and flanges were attached to the steel connecting pipes to attach to the blocks, designed to avoid any changes in diameter, obstructions, cavities or leakages along the length of the test pipe. Pressure ripple was generated using a rotary valve designed to give leakage pulses of very short duration (about 1 msec) as it rotates. This gave a peak-to-peak pressure ripple amplitude of between 0.5 and 2 bar, with stable harmonics of pressure ripple from its fundamental frequency (10 - 50 Hz) to about 5 kHz. In this case it was set to a fundamental frequency of 50 Hz. A typical harmonic amplitude spectrum is shown in figure 2. Other parameters are listed in table 1.

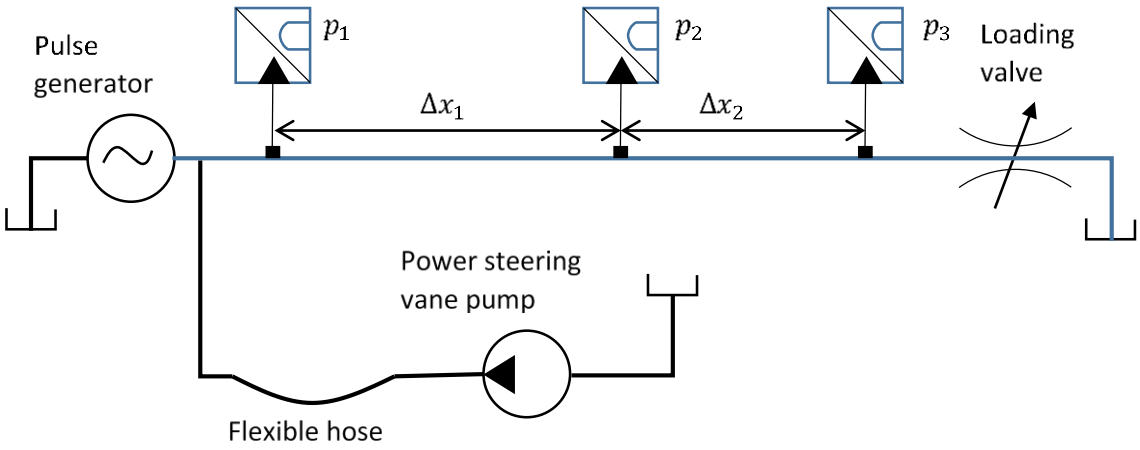

Figure 1. Simplified schematic of test rig

Table 1. Test parameters

Flowrate	11 L/min
Pipe internal diameter	10 mm
Pipe wall thickness	2.5 mm
Distances between transducers	0.670 m, 0.524 m
Sample rate	50 kHz
Data acquisition delay between channels	4 µs

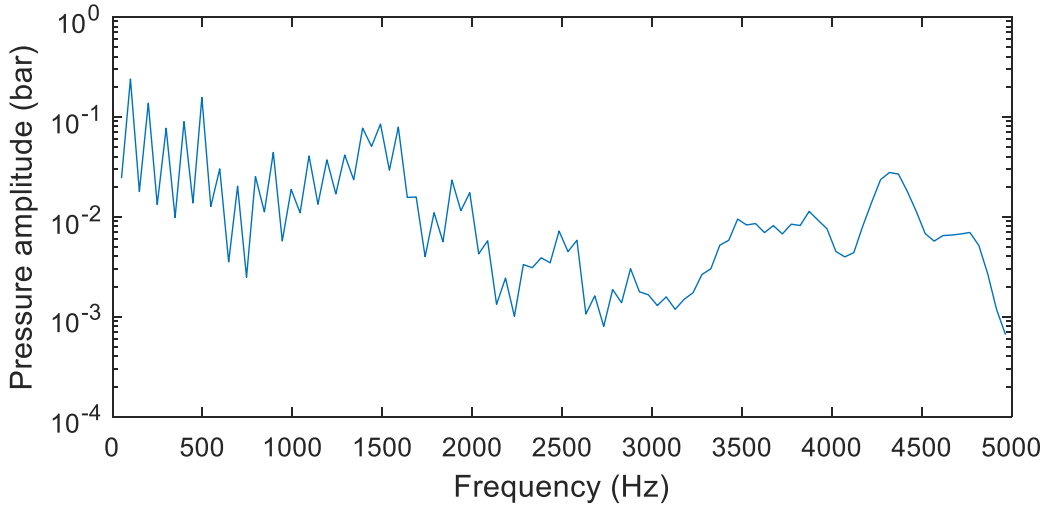

Figure 2. Typical pressure amplitude spectrum for 40 bar mean pressure

Frequency domain method

Considering pressure transducer 2 as the datum position, and defining F and G as the pressure waves at this point travelling in the forward and reverse directions, then [5]:

$$P_1 = Fe^{\gamma\Delta x_1} + Ge^{-\gamma\Delta x_1} \quad (1)$$

$$P_2 = F + G \quad (2)$$

$$P_3 = Fe^{-\gamma\Delta x_2} + Ge^{\gamma\Delta x_2} \quad (3)$$

Equations 1-3 can be combined to eliminate F and G, and rearranged to give

$$P_1\left(e^{\gamma\Delta x_2} - e^{-\gamma\Delta x_2}\right) - P_2\left(e^{\gamma(\Delta x_1+\Delta x_2)} - e^{-\gamma(\Delta x_1+\Delta x_2)}\right) + P_3\left(e^{\gamma\Delta x_1} - e^{-\gamma\Delta x_1}\right) = 0 \quad (4)$$

Or $P_1 \sinh\gamma\Delta x_2 - P_2 \sinh\gamma(\Delta x_1 + \Delta x_2) + P_3 \sinh\gamma\Delta x_1 = 0$ (5)

Where the wave propagation coefficient $\gamma = \frac{j\omega}{c}\sqrt{N}$, (6)

the speed of sound $c = \sqrt{\frac{B_{eff}}{\rho}}$, (7)

the viscous friction function $N = \left(1 - \frac{2J_1(z)}{zJ_0(z)}\right)^{-1}$ where $z = j\sqrt{j\alpha}$, (8)

And non-dimensional frequency $\alpha = \frac{r^2\omega}{\nu}$. (9)

This assumes that the pressure fluctuations are small enough that variations in the effective bulk modulus B_{eff} and density ρ are negligible over the range of fluctuations; this may cause inaccuracies at low pressures when aeration and cavitation become significant. c is the asymptotic value of the phase velocity c_P as $\alpha \to \infty$. Viscosity has the effect of introducing frequency-dependent attenuation (which depends on the imaginary part of $\sqrt{N}$) and a reduction in phase velocity c_P at low frequency, given by

$$\frac{c_P}{c} = \frac{1}{\Re(\sqrt{N})} \quad (10)$$

The variation of phase velocity with non-dimensional frequency is shown in figure 3. For the tests reported here, viscosity ν ranged from 17 to 48 cSt and frequency ranged from 50 to 5000 Hz, giving a range of α from 650 to 1.8×10^5 and $\frac{c_P}{c}$ from 0.95 to 0.997. This is a small but significant variation in phase velocity, and is fully accounted for in the proposed methods.

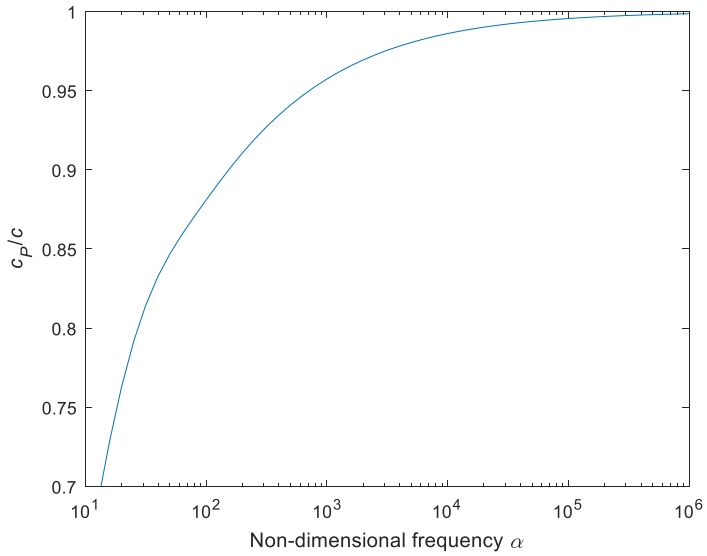

Figure 3. Variation of phase velocity with non-dimensional frequency

For non-zero mean fluid velocity u, provided that $u \ll c$, γ can be approximated to [3, 15]:

$$\gamma_F \approx \frac{j\omega}{c+u}\sqrt{N} = \frac{\gamma}{1+\frac{u}{c}} \approx \gamma\left(1-\frac{u}{c}\right) \approx \gamma - \frac{j\omega u}{c^2} \text{ in the positive } x \text{ direction } (F \text{ wave}) \quad (11)$$

$$\text{And } \gamma_G \approx \frac{j\omega}{c-u}\sqrt{N} = \frac{\gamma}{1-\frac{u}{c}} \approx \gamma\left(1+\frac{u}{c}\right) \approx \gamma + \frac{j\omega u}{c^2} \text{ in the negative } x \text{ direction } (G \text{ wave}). \quad (12)$$

Equation (4) then becomes

$$P_1 e^{j\omega\frac{u}{c^2}\Delta x_2}\left(e^{\gamma\Delta x_2} - e^{-\gamma\Delta x_2}\right) - P_2 e^{j\omega\frac{u}{c^2}(\Delta x_2 - \Delta x_1)}\left(e^{\gamma(\Delta x_1+\Delta x_2)} - e^{-\gamma(\Delta x_1+\Delta x_2)}\right) +$$
$$P_3 e^{-j\omega\frac{u}{c^2}\Delta x_1}\left(e^{\gamma\Delta x_1} - e^{-\gamma\Delta x_1}\right) = 0 \quad (13)$$

$$\text{Or } P_1 \sinh\gamma\Delta x_2 - P_2 e^{-j\omega\frac{u}{c^2}(\Delta x_1)} \sinh\gamma(\Delta x_2 + \Delta x_1) + P_3 e^{-j\omega\frac{u}{c^2}(\Delta x_2+\Delta x_1)} \sinh\gamma\Delta x_1 = 0 \quad (14)$$

Effectively this represents a time delay applied to the middle and downstream transducer equal to the change in wave propagation time due to the mean velocity.

In many multi-input data acquisition systems, the channels are not sampled synchronously but are scanned with a small time delay τ between each channel. This can easily be compensated for by multiplying each pressure signal by $e^{-j\omega(n-1)\tau}$ where n is the channel number.

Because of approximations, incorrect fluid properties and experimental errors this function will not be zero but will be a small value ε.

$$\varepsilon = P_1 \sinh\gamma\Delta x_2 - P_2 e^{-j\omega\frac{u}{c^2}(\Delta x_1)} \sinh\gamma(\Delta x_2 + \Delta x_1) + P_3 e^{-j\omega\frac{u}{c^2}(\Delta x_2+\Delta x_1)} \sinh\gamma\Delta x_1 \quad (15)$$

The sum-of-squares error over M frequencies can be computed. Here it is normalised by dividing by the sum-of-squares of the pressure amplitudes as in equation (16).

$$E = \sum_{i=1}^{M} \frac{|\varepsilon_i|^2}{|P_{1,i}|^2 + |P_{2,i}|^2 + |P_{3,i}|^2} \quad (16)$$

By finding the minimum of this summation, the speed of sound c can be estimated. In [5] a method for estimating confidence limits is given. This is not statistically precise because of the non-linearity of equation (15), but it gives a valuable indication of the precision. There may also be systematic errors or biases due to factors such as incorrect fluid viscosity and non-uniformities (small cavities or obstructions) in the internal cross section of the pipeline. The latter is unavoidable at the pressure transducers because of their flat diaphragms which cannot follow the internal curved surface of the tube precisely, but this is expected to be a very small effect.

Estimation of calibration factors

The error ε is very sensitive to the ratios of pressure transducer calibration factors, so it is feasible and practicable to estimate two of the three calibration factors at the same time as the speed of sound. This may be especially valuable for piezoelectric pressure transducers which are commonly used for fluid-borne noise measurements but which can only measure changes in pressure as the charge due to the mean pressure leaks away over time. Such transducers are difficult to calibrate by conventional static loading techniques and require specialist techniques. Calibration is likely to drift over time, and they are usually returned to the manufacturer or a specialist for periodic calibration. Calibration may also be affected by installation torque and stresses due to misalignment. The method presented here may provide a convenient means for in-situ calibration, as well as for online detection of faults or drifts in the transducers and instrumentation. It is not possible to estimate all three transducer calibration factors however; one of the three has to be fixed as a reference, and essentially the ratios of two transducer calibration factors to this reference value are estimated.

Results

Figure 4 shows the error, (a) over a very broad range of c, and (b) over a narrow range close to the minimum. It can be seen that the minimum is very clearly defined and the error is extremely small at this point, giving an estimated speed of sound of 1344.3 m/s. The estimated 95% confidence limits (using the approximate method described in [5]) are +/- 0.10%, or 1343.0 to 1345.6m/s.

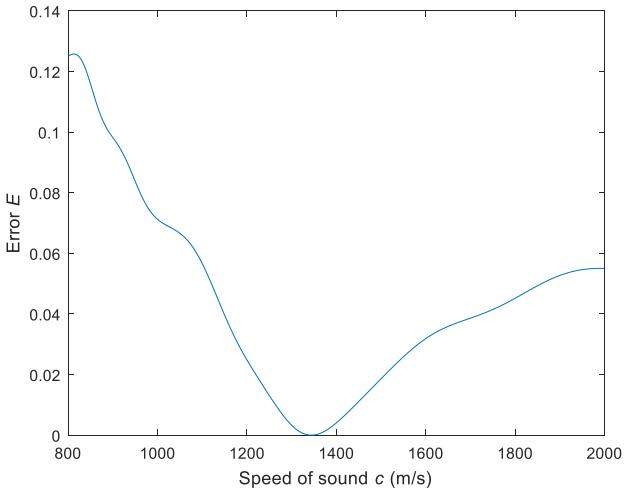

(a) broad range of c

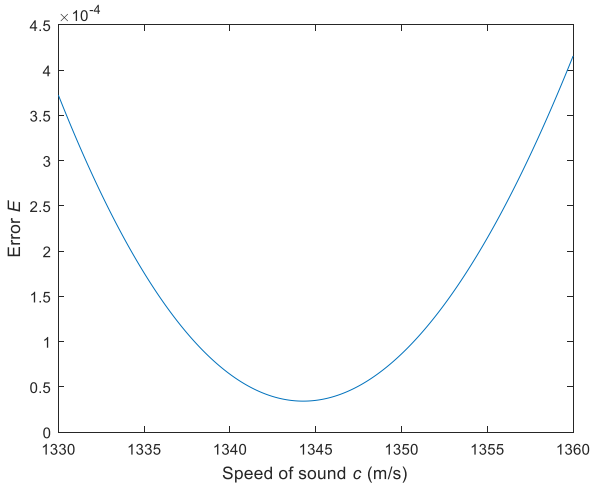

(b) close to the minimum

Figure 4. Error E vs speed of sound, at 40 bar, 35°C.

Assuming a fluid density of 820 kg/m^3, this corresponds to an effective bulk modulus of 14820 bar. Equation (17) defines the effective bulk modulus allowing for the effect of wall compliance and air bubbles. Equation (18) is the thick-wall approximation used for the effect of pipe wall compliance [16 Pearsall]; this assumes that the pipe is unconstrained along its length, but the difference due to assumption of different constraints would be very small (< 0.2% in this case).

$$\frac{1}{B_{eff}} = \frac{1-\phi}{B_f} + \frac{1}{B_w} + \frac{\phi}{kP_{abs}} \tag{17}$$

$$B_w = \frac{E_w}{2\left(\frac{d_o^2+d_i^2}{d_o^2-d_i^2}+\nu_w\right)} \tag{18}$$

Using these equations and neglecting the effect of air bubbles ($\phi = 0$), the estimated isentropic tangent bulk modulus of the fluid B_f is 15580 bar, which is in the expected range.

Figure 5 shows an example of isosurfaces of error E corresponding to the result in figure 4 but for changes in c and calibration factor ratios. The isosurfaces are shaped like ellipsoids, with a ratio of minor axis width to major axis width of about 1:5, with the minor axis offset by a small angle from the speed of sound (vertical) axis. This flattening suggests that the speed of sound estimate is about 5 times as precise as the two calibration estimates. Because the isosurfaces are not strongly elongated, skewed or crescent-shaped, and because there are no other local minima in close proximity, the minimum is easily located using simple optimisation techniques.

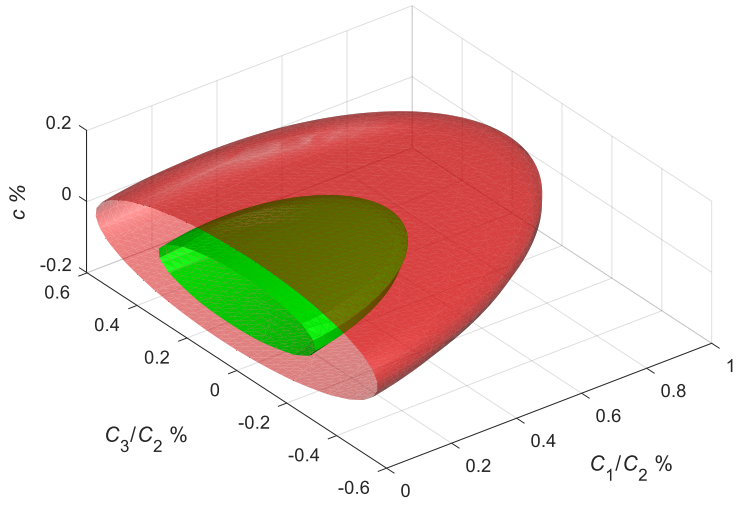

Figure 5. Isosurfaces of error E for changes in speed of sound c, calibration factor ratios C_1/C_2 and C_3/C_2, with percentage change in parameters shown relative to the point of minimum error. Green (inner): $E = 3.6 \times 10^{-5}$; Red (outer): $E = 4 \times 10^{-5}$. Surfaces halved for clarity.

Figure 6 shows the variation of estimated speed of sound with temperature, for three mean pressures. In these tests the calibration factors for the first and third transducers have also been estimated. The speed of sound reduces approximately linearly with temperature, and increases slightly with pressure. This is because the fluid bulk modulus decreases with temperature and increases with pressure (density has similar but smaller variations). Error bars are shown, based on the estimated 95% confidence range. It can be seen that the ranges of the error bars are much smaller than the variations due to temperature and pressure.

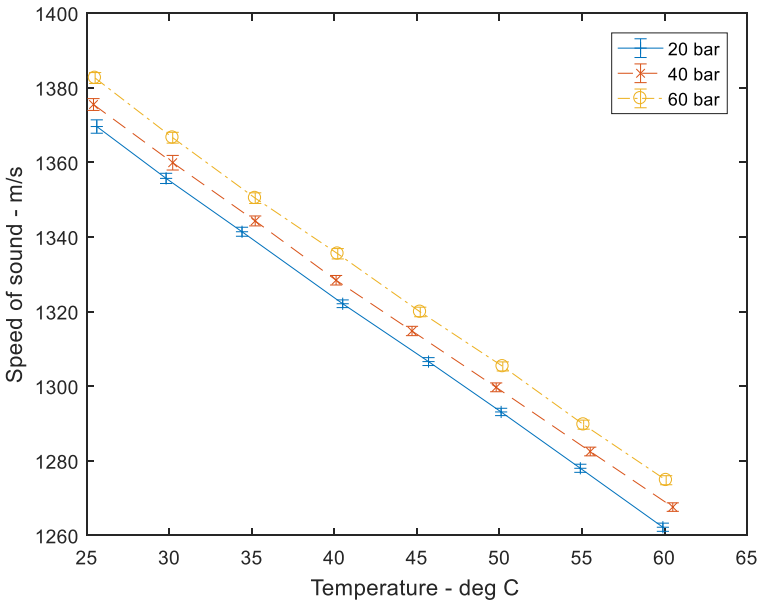

Figure 6. Variation of estimated speed of sound with temperature and pressure

The fluid's isentropic tangent bulk modulus was estimated from these results using equation (7) to obtain the effective bulk modulus, and equations (17) and (18) to estimate the fluid bulk modulus,

assuming no air bubbles were present. The fluid density was required in equation (17) to estimate the bulk modulus; this was measured at atmospheric pressure and two temperatures. Linear interpolation was used to estimate density at other temperatures, and a correction for pressure of 0.006%/bar was used (the latter based on an assumed secant bulk modulus of 16700 bar; this is approximate, but the corrections are very small). There is some uncertainty in the density values because of measurement error and uncertainty in the variation with temperature and pressure. The total uncertainty in density was estimated to be +/- 0.5%, giving a corresponding increase in the fluid bulk modulus uncertainty. Results are shown in figure 7. The bulk modulus is of the expected range for mineral oil based fluids [11] and shows the expected trends, decreasing significantly and approximately linearly with temperature and increasing slightly with pressure.

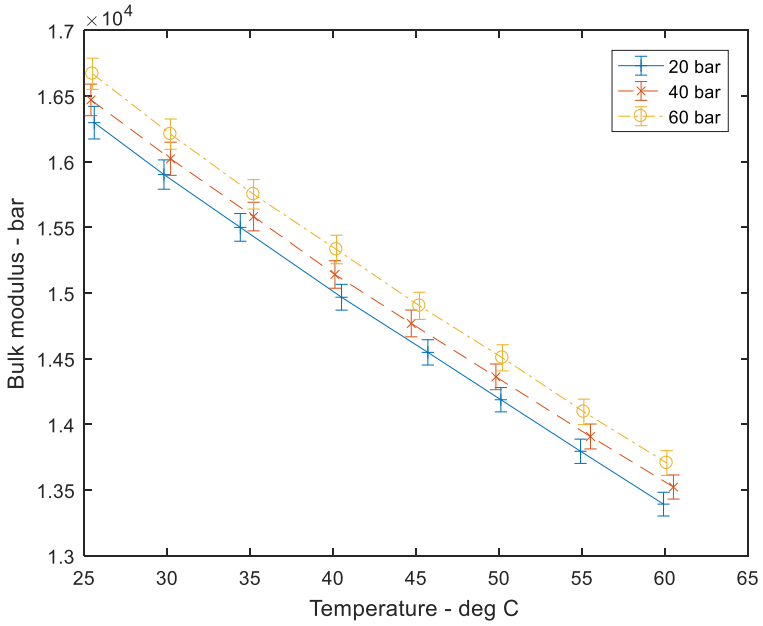

Figure 7. Variation of estimated isentropic tangent bulk modulus of fluid with temperature and pressure

For comparison with estimated pressure transducer calibration factor ratios, ratios of calibration factors were also measured by mounting the transducers in a common block with all three at the same axial position. The same rotary valve was used for pressure ripple generation. The sums of the squares of the harmonic amplitudes were evaluated, from which the ratios of the calibration factors relative to transducer 2 were calculated. These measured calibration ratios were found to be repeatable with a variation of less than 0.1% at a particular pressure and temperature condition. Little variation (<0.2%) with temperature was observed over the range of 37C to 57C.

Figure 8 shows the variation of calibration factor ratios with pressure, estimated in conjunction with the speed of sound using the proposed method (labelled 'inline'), and by mounting them in a common block, for an approximately constant temperature of 55-57°C. 'Inline' estimates were taken before and after the 'common block' tests, and transducers 2 and 3 were removed and reinstalled between the 'inline, before' tests, the 'common block' tests and the 'inline, after' tests. Error bars are shown for the 'inline' estimates, based on the estimated 95% confidence range, and the 'common block' estimates, based on the sum-of-squares error between the harmonic values from the two transducers. An increase in C_1/C_2 and C_3/C_2 with pressure is apparent in all cases, and this is most marked for

C_3/C_2, with changes of up to 5%. This may be due to an increase in the calibration factors C_1 and C_3, or a decrease in C_2. Differences of up to 5.5% are apparent between the C_3/C_2 'inline, before' and 'common block' data. Furthermore, a consistent difference of about 2% is apparent between C_3/C_2 'inline, before' and 'inline, after'.

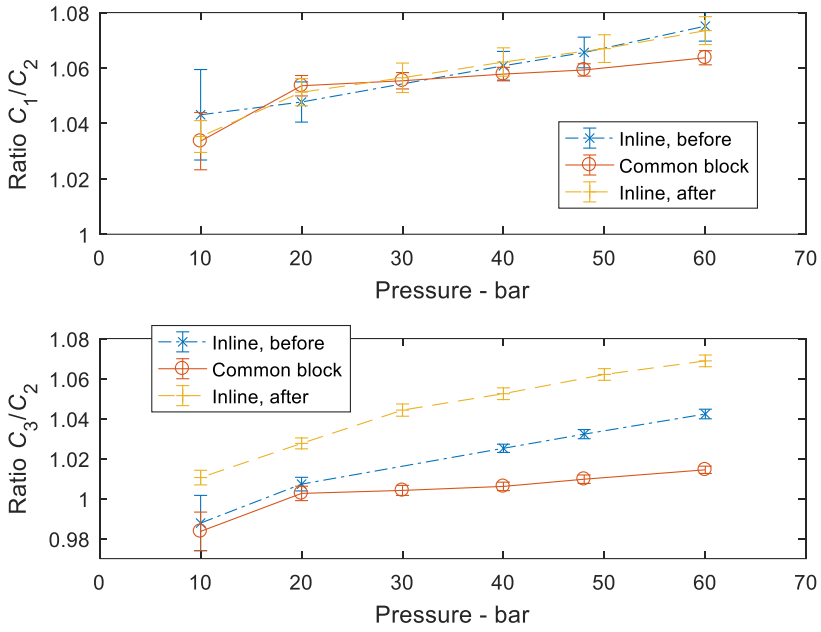

Figure 8. Variation of calibration factor ratios with pressure, measured using a common block, and estimated using proposed method (labelled as 'inline') before and after being removed and replaced for 'common block' test.

At most conditions the error bars are narrower than the variations in calibration factor ratio. The error bars are wider at low pressure because the pressure ripple signals are weaker, especially at high frequency. These results clearly indicate that the calibration factors for these transducers show significant variations. These differences were repeatable and statistically significant, and may be due to non-linearity of response and changes due to physical stresses on the transducers caused by slight differences in the mounting holes or installation torques. The difference in calibration before and after the 'common block' test did not result in any apparent change in the estimated speeds of sound, because the change in calibration was detected and compensated for automatically by the optimisation process.

These results clearly suggest that in-situ estimates of calibration factor ratios using the proposed method may be considerably more precise than predetermined values. This is likely to result in improved accuracy in the estimated speed of sound. It should also result in improved estimates of flow ripple [3, 17], impedance [14] or transfer matrices [7, 14], all of which use similar pressure transducer configurations and require very precise calibration ratios and speed of sound estimates, but are less sensitive to or independent of the absolute calibration values.

Estimation of viscosity and mean velocity

The fluid viscosity has been estimated using the same method as the speed of sound and calibration factor ratios. The viscosity influences the error function (equation (15)) through the wave propagation coefficient (equations (6)-(9)). An example of the error as a function of speed of sound and kinematic viscosity is shown in figure 9. The boundary of the white oval represents the approximate 95%

confidence limit. The confidence limits are about +/- 0.1% for speed of sound and about +/- 20% for viscosity. The much wider viscosity range and poorer precision is because the wave propagation coefficient γ (and hence the error E) is far less sensitive to viscosity than speed of sound, as the dissipation number β is low (< 0.002) in this example, where $\beta = \frac{\nu T}{r^2}$ and T is the wave transmission time between transducers.

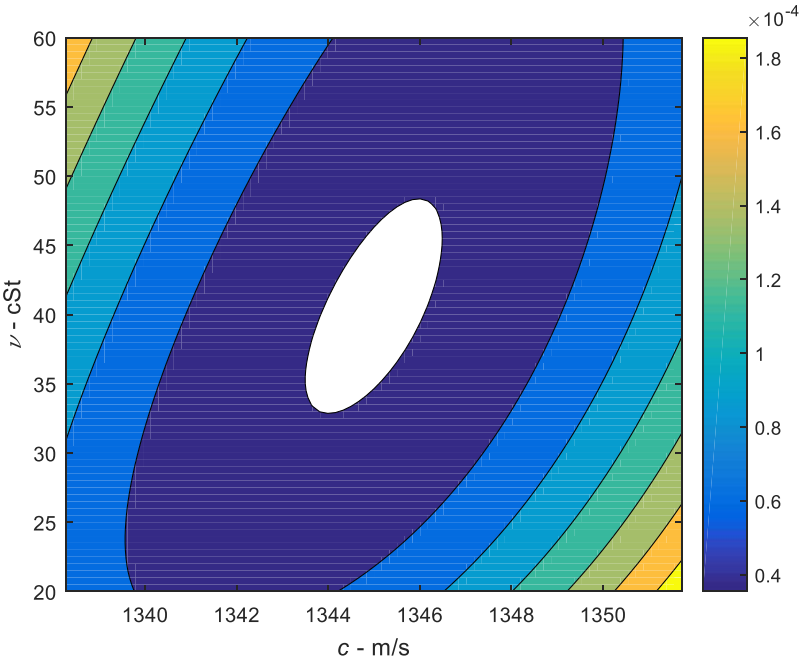

Figure 9. Error contours vs. kinematic viscosity and speed of sound, at 35.2°C, 40 bar

A comparison with viscosity measurements taken using a rheometer (TA Instruments DHR-2) is shown in figure 10. The measured viscosity was adjusted for pressure using an estimated rate of increase of 25% per 100 bar, this being typical of mineral oils [18]. The uncertainty in the viscosity measurements was estimated at +/-10%. The proposed method gives plausible estimates, but has tended to over-estimate the viscosity by up to 40%, with estimated 95% confidence intervals of typically +/- 20%. Despite the limited precision, it may be a valuable tool for fluid condition monitoring in some applications. For much higher dissipation numbers, obtained using a higher viscosity fluid, a smaller diameter or a greater length, it should be possible to estimate viscosity to a better level of precision using this method, as was done by Margolis and Brown [3] for turbulent friction. However for most hydraulic fluid power applications, high dissipation numbers do not commonly occur.

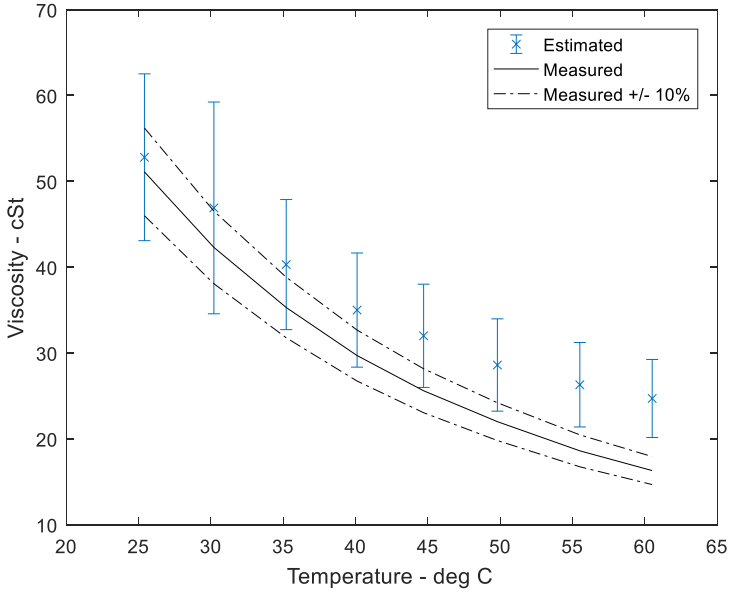

Figure 10. Viscosity estimated using proposed method at 40 bar, and measured using rheometer (pressure correction applied to rheometer measurements)

It is theoretically possible to estimate the mean velocity by the same method, as this also influences the error. However for the tests that have been performed to date, the velocity has been very low (about 2 m/s) relative to the speed of sound (about 1300 m/s) and ε (equation (15)) is relatively insensitive to it. Therefore it is has not been possible to estimate the mean velocity with precision using this method. For conditions of higher velocity or lower speed of sound (e.g. air flow) it may be possible to estimate the velocity with reasonable precision but this has not been done as yet.

Comparison with cross-correlation method

For comparison, a cross-correlation analysis [12] was applied on the same data, using the first and third pressure transducers. The cross-correlation function is shown in figure 11(a) for delays τ from 0 to 2 ms. A peak is apparent at about 0.9 ms; this peak is expanded in figure 11(b) and plotted against speed of sound, given by $c = \frac{\Delta x}{\tau}$. This gives an apparent speed of sound of 1300 m/s. The resolution is poor (~15 m/s or 1.1%); this depends on Δx (1.2 m) and the sample rate (50 kHz), and could be improved by increasing these parameters. The location of the peak can also be identified more precisely by using cubic splines, as shown.

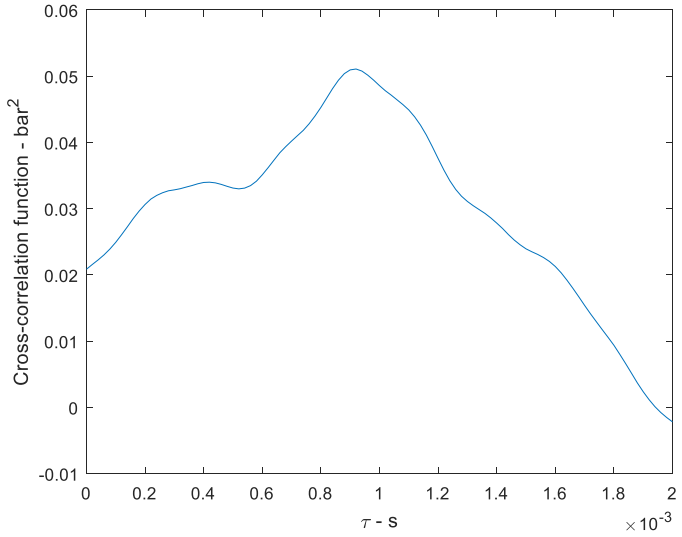

(a) Wide range, plotted versus delay

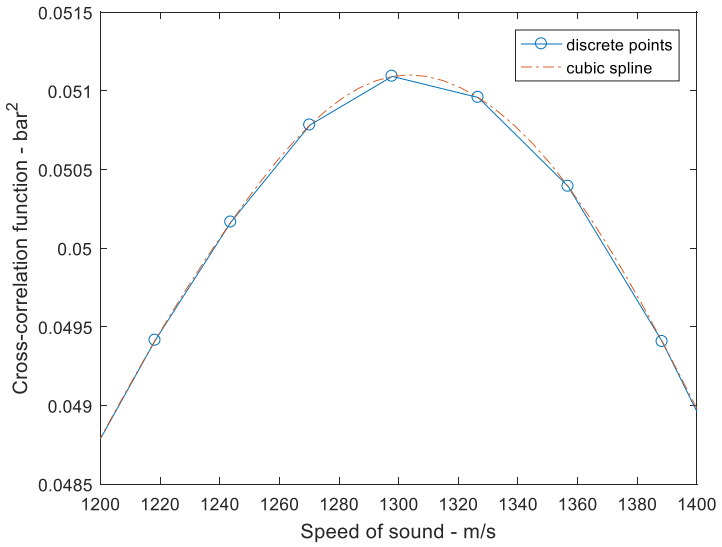

(b) Narrow range near peak, plotted versus equivalent speed of sound

Figure 11. Cross correlation results using same data as figure 3, outer pair of transducers

A comparison between the cross correlation method and the proposed method is shown in figure 12. The trends are similar but the cross correlation results are about 40 m/s (3%) lower than the results obtained using the proposed method. The difference is likely to be due to inaccuracies in the cross correlation method. Results using the cross-correlation method are influenced by reflections, which may give multiple, overlapping or skewed peaks. This is especially so if a partial reflection occurs just beyond the downstream transducer as is the case here, which would be expected to increase the apparent delay and reduce the estimated speed of sound. Also viscous friction effects are ignored in the cross-correlation method and this results in a slight under-estimate; neglecting viscous friction in the proposed method was found to reduce the estimated speed of sound by about 0.7% in this case. The poor resolution of the conventional cross-correlation method is apparent, and a smoother variation is obtained using cubic splines to locate the peak, but the agreement with the proposed

method is not improved. Error bars are not shown for the cross correlation results as it is not clear how large the uncertainty is.

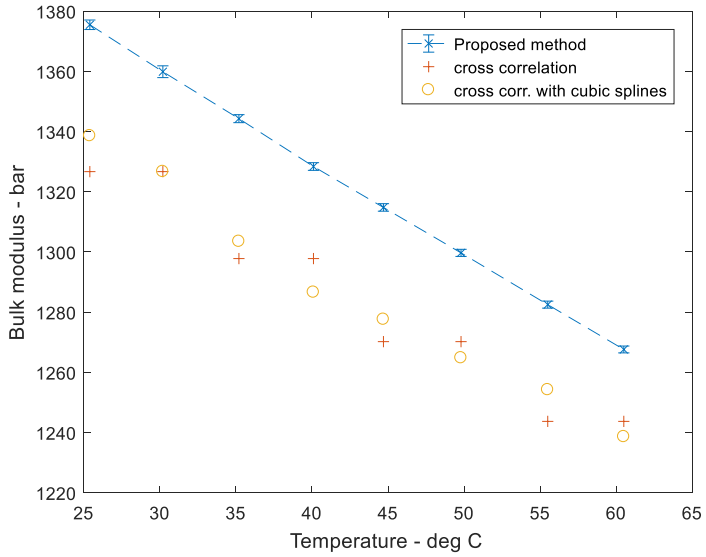

Figure 12. Comparison between the cross correlation method and the proposed frequency domain method, 40 bar

Time domain method

The frequency domain method described above cannot provide instantaneous results as it is necessary to capture a significant block of data (typically several seconds), track the frequency of the pressure ripple source, perform a fast-Fourier transform, and apply a search algorithm to find the minimum error using a computationally intensive error function. Thus there is necessarily a delay of several seconds between the measurements and the estimate. In most situations this is not a problem, but in some situations near-instantaneous tracking of the speed of sound and calibration factors may be needed. Thus a time-domain alternative with less inherent delay is sought. Two methods are presented here, both based on the same error function:

1. a 'block' method where error minimisation is performed for a block of data of typically a few seconds;
2. a 'dynamic' method where the estimate is updated at each sample interval.

The exponential terms in equation (14) can be rearranged to represent a pure delay of time T and a frequency dependent friction term. For example,

$$e^{-\gamma_F \Delta x} = e^{-j\omega T} e^{-j\omega T\left(\sqrt{N}-1\right)} \tag{19}$$

Where $T = \frac{\Delta x}{c+v}$.

An exact time-domain expression for the frequency dependent friction term $e^{-j\omega T\left(\sqrt{N}-1\right)}$ is not available, and an approximation is needed. Johnston [19] and Johnston et al [20] developed two variants of a time-domain transmission line method (TLM) for modelling unsteady flow in tubes. In these methods, wave propagation in the two directions was represented using a pure delay together

with a filter or weighting function to approximate the frequency dependent friction term $e^{-j\omega T(\sqrt{N}-1)}$. In the 'enhanced' method [20], the following approximation was used.

$$e^{-j\omega T(\sqrt{N}-1)} \approx 1 - \sum_{i=1}^{k} \frac{m_i j\omega T}{n_i + j\omega T} = G(j\omega T) \tag{20}$$

The number of terms k in the summation was between 3 and 7 depending on the accuracy and frequency range required, and the coefficients m_i and n_i were optimised to minimise the error and were functions of dissipation number β, where $\beta = \frac{\nu T}{r^2}$.

This filter or weighting function can easily be applied in time domain computations on sampled data. This can be done efficiently using an infinite-impulse-response (IIR) filter. Equation (20) can be expanded into a rational function (i.e. ratio of polynomials) with numerator and denominator of order k, and transformed into a discrete time filter.

Equation (14) can be transformed to the time domain using this approximation. In this derivation, the mean velocity v and the channel delay τ are omitted for clarity. In order to avoid any time advances (to expedite real-time computation, and so that $G(j\omega T)$ can be implemented), all terms are multiplied by $e^{-\gamma(\Delta x_1 + \Delta x_2)}$.

$$\varepsilon(j\omega) = \frac{1}{2}\left|P_1\left(e^{-\gamma\Delta x_1} - e^{-\gamma(\Delta x_1 + 2\Delta x_2)}\right) + P_3\left(e^{-\gamma\Delta x_2} - e^{-\gamma(2\Delta x_1 + \Delta x_2)}\right) - P_2\left(1 - e^{-2\gamma(\Delta x_1 + \Delta x_2)}\right)\right| \tag{21}$$

Using the approximation in equation (20),

$$\varepsilon(j\omega) = \frac{1}{2}\left|P_1\left(G\left(j\omega\frac{\Delta x_1}{c}\right)e^{-j\omega\frac{\Delta x_1}{c}} - G\left(j\omega\frac{\Delta x_1 + 2\Delta x_2}{c}\right)e^{-j\omega\frac{\Delta x_1 + 2\Delta x_2}{c}}\right) - P_2\left(1 - G\left(2j\omega\frac{\Delta x_1 + \Delta x_2}{c}\right)e^{-2j\omega\frac{\Delta x_1 + \Delta x_2}{c}}\right) + P_3\left(G\left(j\omega\frac{\Delta x_2}{c}\right)e^{-j\omega\frac{\Delta x_2}{c}} - G\left(j\omega\frac{2\Delta x_1 + \Delta x_2}{c}\right)e^{-j\omega\frac{2\Delta x_1 + \Delta x_2}{c}}\right)\right| \tag{22}$$

Transforming this to the time domain,

$$\varepsilon(t) = \frac{1}{2}\left|p_1^A\left(t - \frac{\Delta x_1}{c}\right) - p_1^B\left(t - \frac{\Delta x_1 + 2\Delta x_2}{c}\right) - p_2 + p_2^B\left(t - \frac{2(\Delta x_1 + \Delta x_2)}{c}\right) + p_3^A\left(t - \frac{\Delta x_2}{c}\right) - p_3^B\left(t - \frac{2\Delta x_1 + \Delta x_2}{c}\right)\right| \tag{23}$$

Where:

$p_1^A(t)$ is obtained by digital filtering of $p_1(t)$ using the filter $G(j\omega T)$ with $T = \frac{\Delta x_1}{c}$ and the filter coefficients determined for $\beta = \frac{\nu T}{r^2}$,

$p_1^B(t)$ similarly, but with $T = \frac{\Delta x_1 + 2\Delta x_2}{c}$,

$p_2^B(t)$ with $T = \frac{2(\Delta x_1 + 2\Delta x_2)}{c}$,

$p_3^A(t)$ with $T = \frac{\Delta x_2}{c}$,

and $p_3^B(t)$ with $T = \frac{2\Delta x_1 + \Delta x_2}{c}$. (24)

If the inter-channel sample delay and the effect of the mean velocity are included, equation (23) becomes

$$\varepsilon(t) = \frac{1}{2}\left|p_1^A\left(t - \frac{\Delta x_1}{c+u} + \tau\right) - p_1^B\left(t - \frac{\Delta x_2}{c-u} - \frac{\Delta x_1}{c+u} - \frac{\Delta x_2}{c+u} + \tau\right) - p_2 + p_2^B\left(t - \frac{\Delta x_2}{c-u} - \frac{\Delta x_1}{c+u} - \frac{\Delta x_2}{c+u} - \frac{\Delta x_1}{c-u}\right) + p_3^A\left(t - \frac{\Delta x_2}{c+u} - \tau\right) - p_3^B\left(t - \frac{\Delta x_2}{c-u} - \frac{\Delta x_1}{c+u} - \frac{\Delta x_1}{c-u} - \tau\right)\right| \quad (25)$$

'Block' method

Equation (25) can be used to estimate the speed of sound c by minimising the error ε. This can be done using a summation of the squared errors over N_B samples,

$$E = \sum_{i=1}^{N_B} \frac{|\varepsilon(t_i)|^2}{|p_1(t_i)|^2 + |p_2(t_i)|^2 + |p_3(t_i)|^2} \quad (26)$$

It is a simple optimisation task to minimise this as the error E tends to exhibit a clear minimum with no local minima near to the global minimum, provided that the data are of suitable quality.

In most cases (provided the dissipation numbers are small), the filters $G(j\omega T)$ have little effect and results are insensitive to the precise dissipation numbers and times T used to obtain the filter coefficients. It is not necessary to re-compute the filter coefficients for each change in c, and it has been found to be sufficient to calculate the coefficients once using a representative value of c. For example, for the results reported in this paper the dissipation numbers are between 2×10^{-4} and 9×10^{-4}, and a 10% change in the value of c used for computing the filter coefficients resulted in a change in the final estimate of c of just 0.04%. Indeed, omitting the filters altogether resulted in a change in the final estimate of c of just 0.3%. However for higher dissipation numbers the $G(j\omega T)$ filters are likely to have a more significant effect.

To find the precise point of minimum error requires the application of very small changes to the delays in equation (25). For example, for the conditions used here, a change of 1 m/s in the speed of sound results in a change to the shortest delay in equation (25) of about 0.3 µs – considerably less than the sample period (20 µs). Consequently some form of interpolation between samples is necessary as using the nearest sample would result in step changes to the error instead of a smooth curve. Linear interpolation was found to be sufficient; cubic splines were found to give negligible difference. In addition low-pass digital filtering was found to be necessary, as otherwise high frequency noise was found to distort the error curves. A 4th order Butterworth filter with a bandwidth of 5 kHz was found to work well.

Results

Figure 13 shows the error for a range of speed of sound close to the minimum error point, for the same test data that was used for the frequency domain method in figure 4. The number of filter terms k was chosen to be 5.

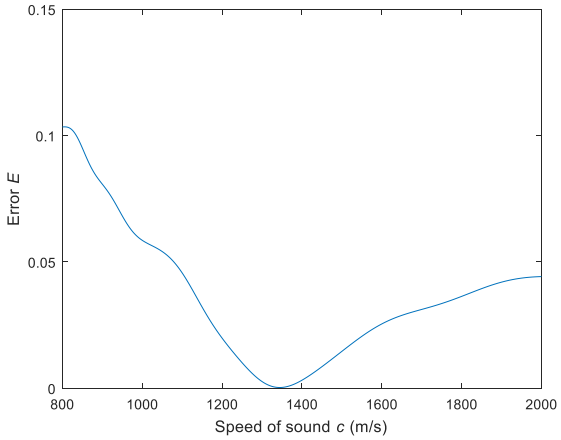

(a) broad range of c

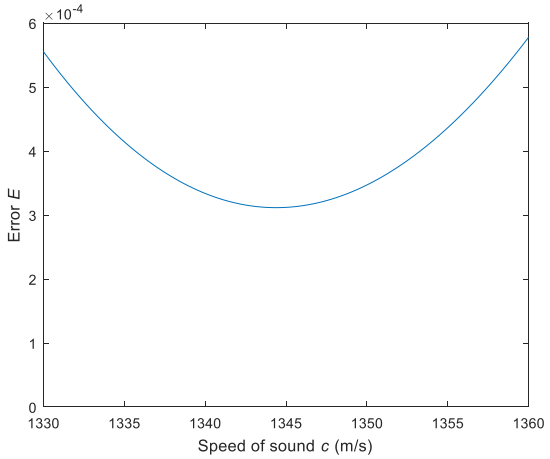

(b) close to the minimum

Figure 13. error E vs speed of sound, 40 bar, 35°C

The minimum error occurs at a speed of sound of 1344.4 m/s. This result is consistent with the value of 1344.3 m/s obtained using the frequency domain method (figure 4), and is well within the 95% confidence interval (1340.8 to 1343.8 m/s) for that test. Whilst the minimum is clear, the minimum error is considerably greater (about six times) than for the frequency domain method. This is probably because of approximations made in equation (20), and because of the interpolation process. Very slight variations in the speed of sound estimate (+/-0.1%) occurred due to changes in the number of terms k between 5 and 7, and due to the interpolation method (linear or cubic spline). The error increases for $k < 5$.

For this time domain method a rigorous statistical confidence interval is difficult to estimate, as the observations (sampled pressure measurements) are not truly independent of each other because of low-pass filtering. The confidence intervals are expected to be wider than for the frequency domain method as the minimum errors are larger.

‘Dynamic’ or ‘real-time’ estimation

The previous methods provide an estimate of speed of sound and calibration factors over the duration of a burst of data. Whilst this is usually likely to be sufficient, the situation may arise where a near-

instantaneous estimate is needed, or changes in the values need to be tracked. This may be the case in the following situations:

- where a precise value of the speed of sound is needed for tuning the frequency of the switching valve in a switched-inertance system in order to get maximum efficiency [2];
- where the instantaneous unsteady flowrate is being measured as described by Johnston et al [8];
- where the speed of sound is used for condition monitoring, such as for detecting aeration;
- where pressure transducer signals are to be monitored for possible faults or calibration changes;
- where the mean velocity is being measured using this method.

Several methods are possible. A very simple recursive least squares (RLS) method is described here to estimate the speed of sound and calibration factors, based on the gradient descent method, where the estimate is updated at each sample time. The algorithm is as follows for speed of sound estimation.

1. Set an initial estimate for the speed of sound.
2. Take sample n of three pressure signals, $p_1(t)$, $p_2(t)$, $p_3(t)$.
3. Compute filtered signals $p_1^A(t)$, $p_1^B(t)$, $p_3^A(t)$, $p_3^B(t)$ and $p_2^B(t)$.
4. Update the normalisation value $W_{n+1} = (1-\psi)W_n + \psi\left(p_1^2(t) + p_2^2(t) + p_3^2(t)\right)$, where ψ is a smoothing factor (0.0001 was used here).
5. If sufficient samples have not been taken to compute delayed values, jump to step 8.
6. Add and subtract a small increment to the speed of sound, $+\delta$ and $-\delta$, and compute the errors ε^+ and ε^- using equation (25).
7. Update the speed of sound using the equation $c_{n+1} = c_n\left(1 + \sigma\frac{\varepsilon^- - \varepsilon^+}{W_{n+1}}\right)$.
8. Repeat steps 2-8 for the next sample ($n \to n+1$).

The weighting factor σ controls the speed of response. A large σ gives a fast response but a noisy result. A small σ gives a slow response but a smoother, more consistent result. The normalisation factor ensures that the speed of response is independent of the magnitude of the pressure signals.

Other parameters such as calibration factors can be estimated within the same time-stepping loop, where increments are added and subtracted as in step 6 from each parameter in turn, errors computed and the parameter updated as in step 7.

Results

Figure 14 shows the estimates of speed of sound and calibration factor ratio for the same data as in figures 4 and 13. The starting values at 0 s were 1300 m/s, 1 and 1 respectively, and $\sigma = 0.01$. A fast response is apparent, with a time constant of less than 0.1 s, and some noise is apparent in the predictions. The noise can be reduced by reducing σ, but this will increase the time constant. After the initial transient the estimated speed of sound shows a slight decrease from 1345 m/s to 1344 m/s with noise of +/- 1 m/s. This is consistent with an observed slight increase in temperature from 35.0°C to 35.4°C over this 10 s period. The average value of 1344.5 m/s is consistent with the values obtained with the 'burst' method (1344.4 m/s) and the frequency domain method (1344.3 m/s). The calibration factor ratios are 1.060 and 1.040 +/- 0.003, also consistent with the frequency domain method.

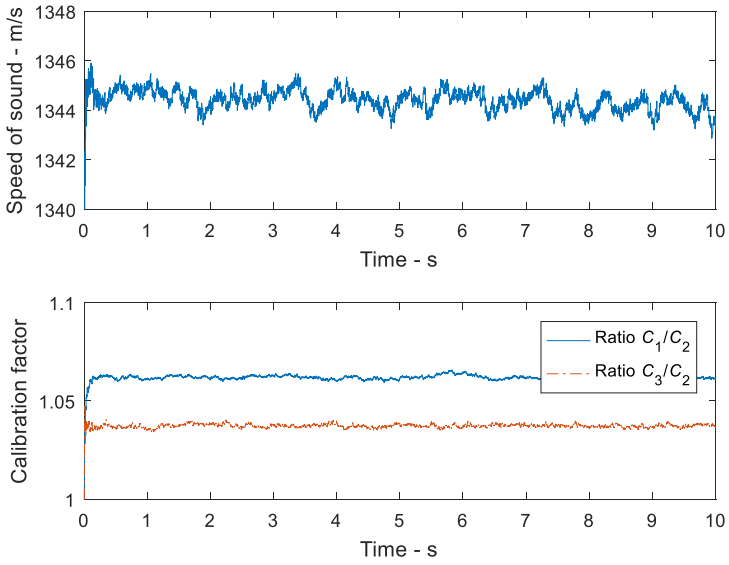

Figure 14. Speed of sound and calibration factor ratios vs. time for 'dynamic' method. 40 bar, 35°C

Aeration

Aeration has a significant effect on the effective bulk modulus and hence the speed of sound [12, 16], as shown by equation (17). This relates to air in the form of gaseous bubbles, which has a very strong effect on the effective bulk modulus; dissolved air has a negligible effect. Pearsall assumed isothermal conditions for the air ($k = 1$), whilst Yu et al assumed adiabatic conditions ($k = \gamma$); the reality is probably somewhere inbetween, but the difference is relatively small compared to uncertainty in the volume fraction ϕ.

The effect of aeration was investigated by pumping about 0.12 L of air into the pump suction line using a bicycle pump, at a roughly constant rate over a period of roughly 6 seconds. It is recognised that this is a crude method, the rate and quantity of air were not tightly controlled, and the air was not distributed evenly through the system, but it was intended just as a qualitative proof of principle.

Results during the aeration process using the 'dynamic' estimation method and 'block' method are shown in figure 15. The air was introduced at a roughly constant rate starting at about 2 seconds and ending at about 8 seconds. The length of line between the pump and first pressure transducer was about 2 m with a fluid transit time of about 1 second. The speed of sound can be seen to be roughly constant for the first four seconds (before the air reaches the transducers) and then falls sharply and clearly before recovering slightly. Both methods show similar results and capture the reduction in speed of sound during the aeration process, with a minimum speed of sound of about 1280 m/s, rising slightly and fluctuating afterwards. This fall of about 2% corresponds to approximately 0.02% of air by volume at the test pressure of 10 bar (expanding to 0.2% at atmospheric pressure). This is a surprisingly low figure as the amount of air pumped in was about 5% by volume at atmospheric pressure. This suggests that most of the air dissolves in the hydraulic fluid in the pump delivery line prior to reaching the pressure transducers. The estimated calibration factors show some spurious but small fluctuations of about 1% during this process.

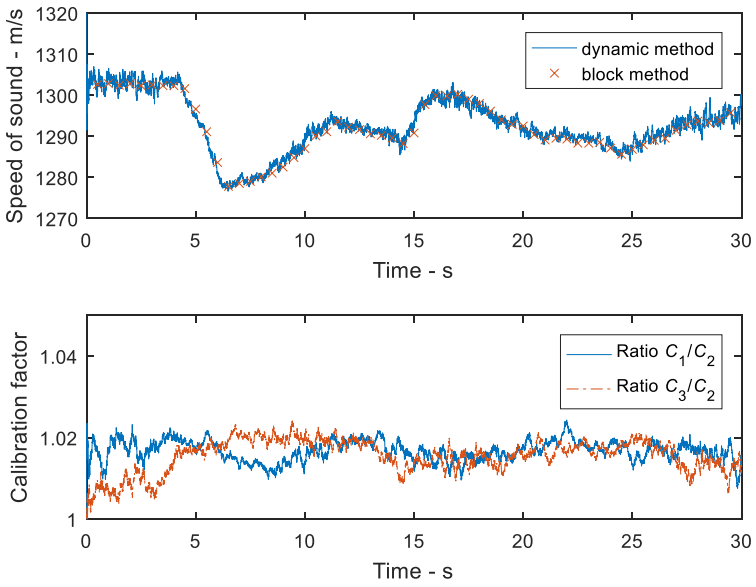

Figure 15. Speed of sound and calibration factors during aeration process. 10 bar, 49°C, $\sigma = 0.01$. 0.5 s blocks used for 'block' method, symbols plotted at end of each block period.

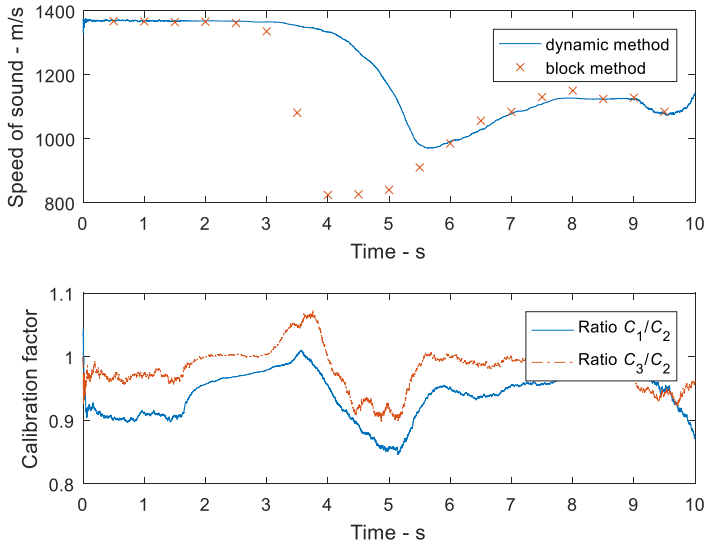

Figure 16. Speed of sound and calibration factors during aeration process. 10 bar, 31°C, $\sigma = 0.01$. 0.5 s blocks used for 'block' method, symbols plotted at end of each block period.

Figure 16 shows results of a similar aeration process at the same pressure of 10 bar but a lower temperature, 31°C. In this case a much larger reduction in speed of sound occurs during the aeration process; however the 'dynamic' method is unable to respond quickly to the sudden drop in speed of sound. The 'block' method shows a minimum speed of sound of about 820 m/s during the aeration process, and both methods show the speed of sound rising to about 1100 m/s afterwards. These figures correspond to approximately 0.07% and 0.025% respectively of air by volume at the test pressure of 10 bar (expanding to 0.7% and 0.25% at atmospheric pressure). It is not clear why more free air remains at 31°C than 49°C; possible reasons are that the amount of air that can be dissolved

in the hydraulic fluid, and the rate of dissolution, may vary with temperature. A detailed investigation of these complex effects is beyond the scope of this paper, but the proposed methods may prove invaluable for further investigation.

More sophisticated tracking methods than the simple RLS method used in the dynamic method may be needed for this rather extreme situation, although increased complexity may incur extra computational effort, limiting the scope for real-time applications.

Similar tests were performed at higher pressures. For pressures greater than about 15 bar, no reduction in speed of sound with aeration was observed, suggesting that all of the air dissolves. Indeed more air can be dissolved at high pressure according to Henry's law. For all load pressures, after aeration, the fluid in the reservoir remained in an opaque, foamed state for several minutes, regardless of whether the measured speed of sound in the high-pressure line was affected by the air. This suggests that after passing through the loading valve downstream of the pressure transducers, at which the point the pressure reduced, the fluid became super-saturated and the air was re-released.

Discussion

It is clear that the proposed methods can provide highly accurate estimates of in-situ speed of sound and calibration factor ratios, in a through-flow pipeline in a working system, without requiring complex pipework or equipment. The accuracy is much higher than can be obtained by other practical means. As the speed of sound and calibration factor ratios are measured in situ in the working system, changes in speed of sound due to different flow conditions, and changes in calibration due to removal and refitting of transducers are avoided. Whilst such calibration changes are likely to be small, their effects can be magnified and they can be significant in precision work. The methods are well suited to real-time monitoring, perhaps for condition monitoring and fault diagnosis.

The time-domain method in particular can be used for real time tuning of digital switched systems to maximise the efficiency. The measured speed of sound and the phase velocity correction shown in figure 3 can be used to set the optimum switching frequency [2].

The quality of the estimates depends on the data quality, which depends on:

- Pressure ripple bandwidth and transducer spacing – best results are obtained if significant pressure ripple energy exists at wavelengths of a similar order to, or shorter than, the transducer spacing.
- Sample rate – results shown here were obtained with a sample rate of 50 kHz; results were poorer, uncertainty increased and errors E larger if the sample rate was reduced.
- Electrical noise, transducer resolution. Low-pass digital filtering can be used to minimise these problems.
- Transducer bandwidths. It is important that all three transducers and their instrumentation have similar amplitude and phase responses over the full bandwidth of the pressure ripple. Phase shifts due to low pass filtering etc. are acceptable provided that they are closely matched for the three transducers.

Almost identical results have been obtained using the frequency domain and time domain methods. There is slightly greater uncertainty in the time domain estimations, because some minor approximations are needed. However the computation is rather simpler in the time domain as only basic arithmetic operations are needed, whereas complex trigonometric, hyperbolic and Bessel functions are needed in the frequency domain.

It is possible to simplify both the frequency and time domain methods by neglecting viscous friction and assuming inviscid conditions, resulting in faster computation. This would produce a slight under-estimate of the speed of sound (because the reduction in phase velocity due to viscosity shown in figure 3 is not being allowed for) and an increase in uncertainty. The magnitude of error that this would produce depends on the dissipation number and the predominant pressure ripple spectral content; generally a high dissipation number and a predominantly low frequency spectrum will produce most error. For the results presented here, neglecting viscous friction results in a reduction of about 0.7% in the estimated speed of sound and an increase of the estimated uncertainty from about 0.1% to about 0.25% (note: this is an approximate statistical measure of uncertainty due to random errors, and does not include systematic errors such as that caused by neglecting viscous friction). For many applications this would be acceptable, but it is recommended if possible to include viscous effects for the increased precision and reduced uncertainty.

The current ISO standard for measuring pump ripple and impedance [21] is based on two pressure transducers and two loading conditions. The previous ISO standard and current British ISO standard "secondary source" method [1] had the option of using three transducers, which has a number of advantages [17]:

- It enables measurement over a much broader frequency range because the situation where the transducers are a half-wavelength apart (at which the equations become ill-conditioned and the accuracy poor) can be avoided by having unequal transducer spacing.
- It provides a measure of error, redundancy, and fault diagnostics.
- It enables accurate measurement of the speed of sound and calibration factors using the proposed methods, which consequently improves the accuracy of the flow ripple and impedance measurements.

Bramley and Johnston [17] proposed that the ISO standard 'two loads' method could be improved considerably, and the disadvantages listed above overcome, by using three transducers. This would increase the complexity of analysis but could greatly improve the accuracy, reliability and confidence in the results. It would make the method compatible with the speed of sound and calibration factor estimation methods proposed here.

Conclusions

The existing ISO standard 3-transducer method for in-situ measurement of speed of sound has been enhanced and extended to enable the in-situ measurement of pressure transducer calibration factors to a high precision. This avoids uncertainty that may arise due to slight changes in calibration during installation or use, and improves the accuracy of the speed of sound measurement. The method highlighted some significant changes in calibration factors due to installation changes, which would be difficult to determine by other means. Speed of sound can be measured to a very high precision, with an estimated 95% confidence band of less than +/-0.1% being achievable. Fluid viscosity and velocity can also be estimated, but the precision is poorer.

A new implementation of the method using time domain analysis has been introduced. This provides the same results as the frequency domain method, but is computationally simpler and facilitates real-time tracking of variations in the speed of sound and calibration factors. This should be valuable for tuning of digital switched hydraulic systems for maximum efficiency, and for condition monitoring.

Further work could be aimed at investigating the sensitivity of transducer calibration to installation stresses, and extending the methods to gas flow, in which accurate estimation of gas velocity may be

feasible. The methods could also be used to investigate the effects of aeration, as shown in some preliminary results here.

Declaration of conflicting interests

The author declares that there is no conflict of interest.

References

[1] BSI, 2015, "BS ISO 10767-1 Hydraulic Fluid Power. Determination of pressure ripple levels generated in systems and components. Method for determining source flow ripple and source impedance of pumps."

[2] Pan, M., Johnston, D.N., Plummer, A.R. and Hillis, A.J., 2013, Theoretical and experimental studies of a switched inertance hydraulic system. Proc. Inst. Mech. Eng., Part I, 228 pp. 12-25

[3] Margolis, D.L. and Brown, F.T., 1976, Measurement of the propagation of long-wavelength disturbances through turbulent flow in pipes. Trans ASME J. Fluids Engng, 70-78

[4] Bolleter, U. 1981, Using transfer function measurements to determine energy propagation in fluid lines, with application to centrifugal pump systems. International Congress on Recent developments in acoustic intensity measurement, France. (Centre Technique des Industries Mechaniques, Senlis, France)

[5] Johnston, D. N., and Edge, K. A., 1991, "In Situ Measurement of the Wavespeed and Bulk Modulus in Hydraulic Lines," Proc. Inst. Mech. Eng., Part I, 205, pp. 191–197.

[6] Johnston, D. N., and Drew, J. E., 1996, "Measurement of Positive Displacement Pump Flow Ripple and Impedance," Proc. Inst. Mech. Eng., Part I, 210, pp. 65–74.

[7] Drew, J. E., Longmore, D.K. and Johnston, D. N., 1996, Measurement of the longitudinal transmission characteristics of fluid-filled hoses, Proc. Inst. Mech. Eng., Part I, 211, pp. 219-228

[8] Johnston, D.N., Pan, M., Kudzma, S., Wang, P., 2014, "Use of Pipeline Wave Propagation Model for Measuring Unsteady Flow Rate", Trans. ASME, J. Fluids Engng, 136,

[9] Johnston, D.N., Way, T.M., Cone, K.C., 2010, Measured Dynamic Properties of Flexible Hoses, Trans. ASME, J. Vibration & Acoustics, 132

[10] ISO, 2000, "15086-2 Hydraulic fluid power -- Determination of the fluid-borne noise characteristics of components and systems -- Part 2: Measurement of the speed of sound in a fluid in a pipe"

[11] Karjalainen, J-P., Karjalainen, R., Huhtala, K. and Vilenius, M, 2011. "Comparison of measured and predicted dynamic properties of different commercial hydraulic fluids", The 12th Scandinavian Int. Fluid Power Conf., May 18-20, Tampere, Finland

[12] Yu, J., Chen, Z. and Lu, Y., 1994, The variation of oil effective bulk modulus with pressure in hydraulic systems. Journal of dynamic systems, measurement, and control 116.1, pp. 146-150.

[13] Yu, J. and Kojima, E., 2000, Methods for measuring the speed of sound in the fluid in fluid transmission pipes. SAE Technical Paper No. 2000-01-2618.

[14] ISO, 2008, "15086-3 Hydraulic fluid power -- Determination of the fluid-borne noise characteristics of components and systems -- Part 2: Measurement of hydraulic impedance"

[15] Wylie EB and Streeter VL. Fluid transients. Revised ed. New York and London: McGraw-Hill, 1978.

[16] Pearsall, I.S., The velocity of water hammer waves, Proc IMechE, Part A, 1990, 204(A1), pp. 41-46

[17] Bramley, C. and Johnston, D.N.,2017, Comparison of methods for measuring pump flow ripple and impedance, Symposium on Fluid Power and Motion Control, FPMC2017-4223, Sarasota, Oct.

[18] OELCHECK, Viscosity, https://en.oelcheck.com/wiki/Viscosity, accessed 3rd August 2018.

[19] Johnston DN. The transmission line method for modelling laminar flow of liquid in pipelines. Proc IMechE, Part I: J Systems and Control Engineering 2012; 226(5): 586–597.

[20] Johnston, D.N., Pan, M. and Kudzma, S., An enhanced transmission line method for modelling laminar flow of liquid in pipelines, Proc IMechE, Part I: J Systems and Control Engineering 2014; 228(4): 193-206

[21] ISO, 2015, "10767-1 Hydraulic Fluid Power - Determination of pressure ripple levels generated in systems and components - Part 1: Method for determining source flow ripple and source impedance of pumps."

Appendix

Notation

B_f Isentropic tangent bulk modulus of fluid

B_{eff} Effective isentropic tangent bulk modulus

B_w Bulk modulus correction due to wall compliance

c Speed of sound

c_P Phase velocity

C_1-C_3 Calibration factors for pressure transducers 1-3

d_i Inner diameter of pipe

d_o Outer diameter of pipe

E_w Young's modulus of pipe wall

E Sum of squares error

F, G Fourier transformed pressure waves travelling in the forward and reverse directions, respectively

G Weighting function

k Polytropic constant

m_i, n_i Coefficients of the i^{th} weighting function

M Number of frequency points in summation

n Timestep index

N Viscous friction function

N_B Number of samples in block

p_1-p_3 Pressures measured at transducers 1-3

p_{1-3}^A, p_{1-3}^B Filtered pressures

P_1-P_3 Fourier transformed pressures measured at transducers 1-3

P_{abs} Mean absolute pressure

r Pipe inner radius

T Wave transmission time

u Mean fluid velocity

W Normalisation factor

z Complex coefficient

α Non-dimensional frequency

β Dissipation number

γ Wave propagation coefficient

γ Ratio of specific heats

δ Increment to speed of sound

$\Delta x_{1,2}$ Spacing between transducers

ε Error

ν Kinematic viscosity

ν_w Poisson's ratio of wall

ρ Fluid density

σ Weighting factor

τ Sample delay between channels

τ Cross correlation delay

ψ Smoothing factor

ϕ Free air volume fraction

ω Angular frequency